

Thermal stability and thermoelectric properties of Cd-doped nano-layered Cu_2Se prepared using NaCl flux method

Jianhua Lu(陆建华), Decong Li(李德聪), Wenting Liu(刘文婷), Lanxian Shen(申兰先), Jiali Chen(陈家莉), Wen Ge(葛文), and Shukang Deng(邓书康)

Citation: Chin. Phys. B, 2020, 29 (**12**): 127403. DOI: 10.1088/1674-1056/abbbf5
Journal homepage: http://cpb.iphy.ac.cn; http://iopscience.iop.org/cpb

What follows is a list of articles you may be interested in

Specific heat in superconductors

Hai-Hu Wen(闻海虎)
Chin. Phys. B, 2020, 29 (**1**): 017401. DOI: 10.1088/1674-1056/ab5a3d

Synthesis, physical properties, and annealing investigation of new layered Bi-chalcogenide $LaOBiHgS_3$

Yi Yu(于一), Chunchang Wang(汪春昌), Liang Li(李亮), Qiuju Li(李秋菊), Chao Cheng(程超), Shuting Wang(王舒婷), Changjin Zhang(张昌锦)
Chin. Phys. B, 2019, 28 (**1**): 017401. DOI: 10.1088/1674-1056/28/1/017401

Thermal stability and electrical transport properties of Ge/Sn-codoped single crystalline β-Zn_4Sb_3 prepared by the Sn-flux method

Hong-xia Liu(刘虹霞), Shu-ping Deng(邓书平), De-cong Li(李德聪), Lan-xian Shen(申兰先), Shu-kang Deng(邓书康)
Chin. Phys. B, 2017, 26 (**2**): 027401. DOI: 10.1088/1674-1056/26/2/027401

Structural stabilities and electrical properties of $Ba_8Ga_{16-x}Cu_xSn_{30}$ single crystals under high temperatures

Jin-Song Wang(王劲松), Feng Cheng(程峰), Hong-Xia Liu(刘红霞), De-Cong Li(李德聪), Lan-Xian Shen(申兰先), Shu-Kang Deng(邓书康)
Chin. Phys. B, 2016, 25 (**6**): 067402. DOI: 10.1088/1674-1056/25/6/067402

Sn-based type-VIII single-crystal clathrates with a large figure of merit

Deng Shu-Kang, Li De-Cong, Shen Lan-Xian, Hao Rui-Ting
Chin. Phys. B, 2012, 21 (**1**): 017401. DOI: 10.1088/1674-1056/21/1/017401

Thermal stability and thermoelectric properties of Cd-doped nano-layered Cu_2Se prepared using NaCl flux method*

Jianhua Lu(陆建华)[1], Decong Li(李德聪)[1,2], Wenting Liu(刘文婷)[1], Lanxian Shen(申兰先)[1], Jiali Chen(陈家莉)[1], Wen Ge(葛文)[1], and Shukang Deng(邓书康)[1,†]

[1] *Education Ministry Key Laboratory of Renewable Energy Advanced Materials and Manufacturing Technology, Yunnan Normal University, Kunming* 650500, *China*

[2] *Photoelectric Engineering College, Yunnan Open University, Kunming* 650500, *China*

(Received 9 July 2020; revised manuscript received 3 September 2020; accepted manuscript online 28 September 2020)

Cu_2Se is a promising "phonon liquid–electron crystal" thermoelectric material with excellent thermoelectric performance. In this work, Cd-doped $Cu_{2-x}SeCd_x$ ($x = 0$, 0.0075, 0.01, and 0.02) samples were prepared using NaCl flux method. The solubility of Cd in Cu_2Se at room temperature was less than 6%, and a second phase of CdSe was found in the samples with large initial Cd content ($x = 0.01$ and 0.02). Field-emission scanning electron microscopic image showed that the arranged lamellae formed a large-scale layered structure with an average thickness of approximately 100 nm. Transmission electron microscopy demonstrated that doping of Cd atoms did not destroy the crystal integrity of Cu_2Se. A small amount of Cd in Cu_2Se could reduce the electrical and thermal conductivities of the material, thus significantly enhancing its thermoelectric performance. With the increase in Cd content in the sample, the carrier concentration decreased and the mobility increased gradually. Thermogravimetric differential thermal analysis showed that no weight loss occurred below the melting point. Excessive Cd doping led to the emergence of the second phase of CdSe in the sample, thus significantly increasing the thermal conductivity of the material. A maximum ZT value of 1.67 at 700 K was obtained in the $Cu_{1.9925}SeCd_{0.0075}$ sample.

Keywords: thermoelectric material, Cu_2Se doping and second phase, NaCl flux, thermoelectric transfer performance

PACS: 74.72.–h, 72.20.Pa, 81.30.Hd, 81.16.Nd **DOI:** 10.1088/1674-1056/abbbf5

1. Introduction

Reducing energy waste plays an essential role in solving global energy and environmental problems.[1] Thermoelectric materials are a kind of functional materials that could directly realize the mutual conversion between heat and electricity.[2] Thermoelectric power generation has advantages, such as the absence of rotating parts, noise, and liquid or gaseous working medium. The performance of thermoelectric materials is measured using the dimensionless ZT ($ZT = \alpha^2\sigma T/\kappa$) value, where σ is the electrical conductivity; α is the Seebeck coefficient; T is the absolute temperature; and κ is the total thermal conductivity, which is composed of electron thermal conductivity (κ_e) and lattice thermal conductivity.[3] Excellent thermoelectric materials should have high Seebeck coefficient and low conductivity and thermal conductivity.[4] Two conventional methods are used to optimize the ZT value of materials. One method is to optimize the energy band structure of materials through doping, which effectively controls the carrier mobility, carrier concentration, and effective mass of state density and then optimizes the electrical transmission characteristics of materials.[5] The other method is to reduce thermal conductivity through nanostructures or phonon engineering κ.

Cu_2Se is a promising "phonon liquid–electron crystal" thermoelectric material with high electrical transmission performance and very low thermal conductivity. It has attracted much attention in recent years due to its excellent thermoelectric performance ($ZT \approx 2.1$ at 973 K).[6] At approximately 400 K, Cu_2Se undergoes reversible structural transformation, in which the low-temperature α-Cu_2Se phase with monoclinal structure and the space group of $C2/c$ transform into high-temperature β-Cu_2Se phase with cubic structure and space group of $Fm\bar{3}m$.[5] Two different sublattices exist in the crystal structure of $Cu_{2-x}Se$.[7] Se atoms form a rigid sublattice, which provides a crystal channel for the conductive carrier. Cu atoms are disorderly distributed in the rigid anionic sublattice, with a high diffusion coefficient of approximately 10^{-5} cm^2/s.[5] This high diffusion coefficient enables Cu^+ ions to jump continuously from one equilibrium position to another in a short time. In this case, the Cu sublattice behaves like a liquid for the wave propagation to be significantly disturbed. Furthermore, liquid-moving Cu^+ ions introduce additional scattering into the lattice phonons to further destroy the heat propagation or change the phonon transfer, thus shortening the average phonon free path and inhibiting. The

*Project supported by the National Natural Science Foundation of China (Grant Nos. 61864012 and 21701140) and the Program for Innovative Research Team (in Science and Technology) in University of Yunnan Province, China.

†Corresponding author. E-mail: skdeng@126.com

© 2020 Chinese Physical Society and IOP Publishing Ltd

superionic diffusivity of Cu^+ ions is beneficial for reducing the thermal conductivity of Cu_2Se phase at high temperature. However, it has adverse effects on electrical conductivity for low carrier mobility caused by impurity scattering and chemical stability caused by the promotion of Cu^+ ion migration. A high-performance diffusion barrier could be used to stabilize Se evaporation and Cu^+ ion migration. This stability is achieved by appropriate cation or partial doping in nanostructures, which could prevent phonon propagation and limit Cu^+ diffusion across interfaces while allowing carriers to transfer between interfaces.

In 2012, Liu *et al.* reported that the ZT value of Cu_2Se is approximately 1.5 at 1000 K.[8] Therefore, researchers have systematically studied the crystal structure and phase transition characteristics of Cu_2Se and further improved the thermoelectric properties of Cu_2Se materials by optimizing the preparation or doping process. Ag-doped Cu_2Se prepared via spark plasma sintering was recently reported to improve the thermoelectric performance of Cu_2Se under 700 K.[9] The ZT value of Al-doped $Cu_{1.94}Al_{0.02}Se$ compound prepared using ball milling method is up to 2.6 at 1020 K.[10] Zhao *et al.* studied a series of $Cu_2Se_{(1-x)}S_x$ and found that the compound has a heterogeneous structure of α-Cu_2Se and β-Cu_2Se mixture at room temperature. It is converted to β-Cu_2Se single-phase cubic structure at high temperature, and S doping considerably reduces carrier concentration, enhances phonon point defect scattering, and significantly reduces thermal conductivity; the maximum ZT value obtained is 1.65 at 950 K.[11] Besides, the Cu_2Se obtained through C fiber doping[12] and Cu_2Se/CNT[13] hybridization both reached 2.4 at 850 K and 1000 K, respectively, and a ZT value of 2.6 is obtained in $Cu_2Se/CuInSe_2$ nanocomposites[14] at 850 K. The alloying of SnTe and Cd could enlarge the bandgap and reduce the energy separation between the heavy and light valence bands, thereby optimizing the band structure of SnTe and improving the power factor.[15]

Although Cu_2Se thermoelectric materials are experiencing increasing research interest due to the high ZT values, however, the Cu^+ ions in Cu_2Se might deposit from the sample under current, which limits the practical application of Cu_2Se. The main factors causing instability are Se loss at high operating temperatures and electro-migration of Cu, which leads to the expulsion of solid Cu from the material. The reaction between free Cu and loss Se with the electrical contacts of the TE device causes an increased contact resistance, which reduces the generation efficiency and thus limits the practical application of Cu_2Se. In the present work, Cd was doped into nanometer-layered Cu_2Se compounds to optimize the thermoelectric properties on the basis of previous work.

2. Experimental sections

2.1. Synthesis method

The sample was prepared using NaCl flux combined with a slow-melting cooling process. The stoichiometric ratio of $Cu : Se : Cd : NaCl = 2-x : 1 : x : 2.5$ ($x = 0$, 0.0075, 0.01, and 0.02) was used for weighing. The raw materials were high-purity Cu (particle, 99.999%), Se (particle, 99.999%), Cd (particle, 99.999%), and NaCl (particle, 99.999%). After the mixture was weighed, it was sealed in a vacuum quartz tube and heated from 300 K to 1443 K for 3 h. After the mixture was incubated at this temperature for 12 h, it was cooled to 1273 K for 2 h, followed by cooling to 773 K for 120 h. Then, the melt was naturally cooled to room temperature. Finally, NaCl was dissolved in distilled water to separate the crystals.

2.2. Material characterizations

Powder x-ray diffraction (XRD, Ultima IV) with Cu-$K\alpha$ radiation ($\lambda = 1.5403$ Å) was performed to test the crystal structure with a scan angle ranging from 10° to 70° and a step size of 0.02°. The internal microstructures of the samples were analyzed through field-emission scanning electron microscopy (FESEM, SUPRA 55VP), and elemental compositions were qualitatively detected via electron energy dispersive x-ray spectroscopy (EDS, Oxford). The actual contents of each element in the crystal were obtained through electron probe microanalysis (EPMA, HT1720 KMUST). The transmission electron microscopy (TEM) image and corresponding selected area electron diffraction (SAED) pattern were observed using a TEM apparatus (Tecnai G20). The chemical states of each element in the samples were measured via x-ray photoelectron spectroscopy (XPS, K-Alpha+).

2.3. Thermoelectric performance measurement

Thermal conductivity κ was calculated using $\kappa = DC_p\rho$ where D, C_p, and ρ are the thermal diffusivity, specific heat capacity, and density, respectively. D was measured using a laser flash apparatus (Netzsch LFA 457, Germany). Thermogravimetric differential scanning calorimetry (TA Q20) was used to measure the C_p of Cu_2Se. ρ was measured via the Archimedes method. κ_L was calculated using $\kappa = \kappa_L - \kappa_e$ where κ_e is the electrical conductivity calculated using $\kappa_e = L\sigma T$ (L is the Lorenz number). Here, $L = 2.0 \times 10^{-8}$ V^2/K^2 was applied. α and σ were measured from 300 K to 700 K in a vacuum environment. α was obtained through a comparative method by using Konstantin (Ni: 40%) as a reference sample, whose $a(T)$ was known in the measured temperature range. σ was measured using a standard four-point probe method, and DC was maintained at 20 mA. Hall coefficient R_H was measured using the Nanometrics HL5500 Hall system. Carrier concentration n and carrier mobility μ_H were calculated from R_H and σ by

using the following formulas: $n = (1/e)R_H$ and $\mu_H = \sigma R_H$, where e is the electron charge. The uncertainty of the measurements of α, σ, and D was $\sim 5\%$, and the uncertainty of the measured C_p was $\sim 10\%$. The weight loss and melting point of the obtained samples were measured via thermogravimetric differential scanning calorimetry (TGA/HT DSC HSS2) in an open alumina crucible at a heating rate of 10 K/min, and high purity nitrogen was used as the purge gas.

3. Results and discussion

3.1. Structure, composition, and chemical state of elements

Figure 1(a) shows the full spectrum of XPS of the sample $x = 0.0075$. The three energy states of Cu 2p, Se 3d, and Cd 4f appeared in the sample, indicating no other energy states except O and C. Figure 1(b) shows the XPS spectrum of Cd 4f, where the chemical binding energies of Cd $3d_{5/2}$ and Cd $3d_{3/2}$ were located at 405.35 eV and 412.05 eV, respectively, which is the characteristic binding energy of Cd^{2+}.[16] Figure 1(c) shows the XPS spectrum of the Se 3d energy state. In the Se 3d spectrum, the binding energies of Se $3d_{5/2}$ and Se$3d_{3/2}$ peaks were 54.15 eV and 54.95 eV, respectively, and the splitting value is 0.8 eV similar to the reported-2 valence.[17] Figure 1(d) illustrates the XPS spectrum of Cu 2p. The binding energies of Cu $2p_{3/2}$ and $2p_{1/2}$ peaks appeared at 932.9 eV and 952.8 eV, respectively. These binding energies were consistent with those of Cu^+ ions reported in the literature, indicating that the Cu in the system has a +1 valence.[17] Besides, two high binding energy shoulder peaks at 949.5 eV and 934.5 eV were observed in the XPS spectra of Cu, corresponding to the Cu^{2+} chemical displacement in CuO. This finding demonstrated that the Cu_2Se surface was slightly oxidized.

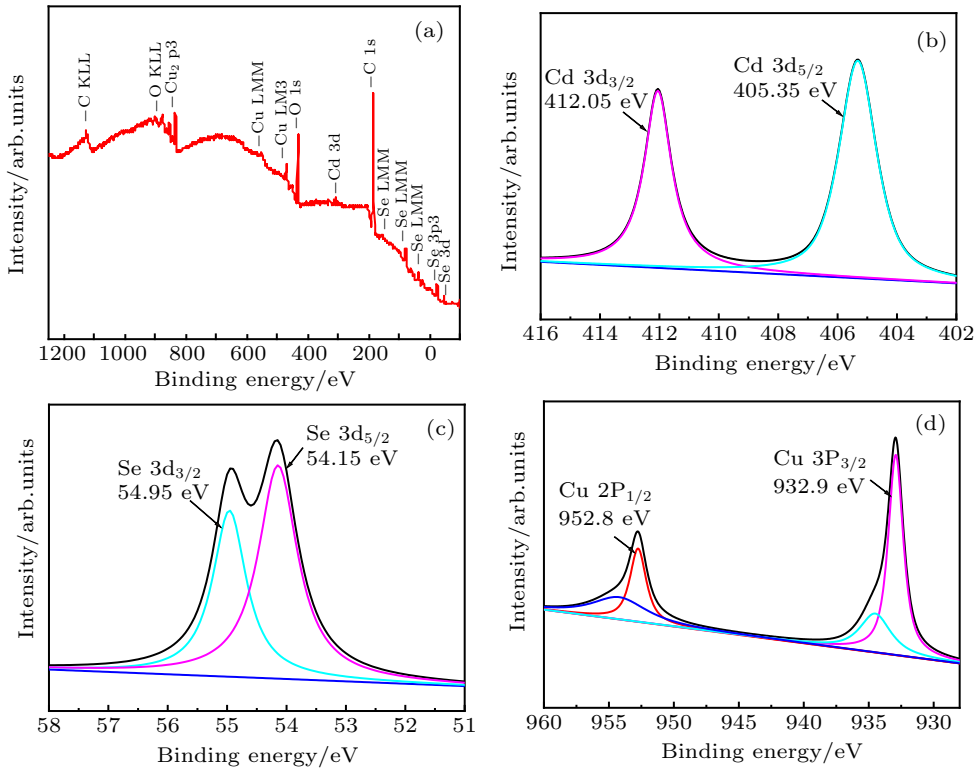


Fig. 1. (a) XPS spectra of the sample $x = 0.0075$, (b) Cd 3d, (c) Se 3d, and (d) Cu 2p.

Figure 2 shows the XRD pattern of all samples at room temperature. For the samples with low initial Cd content ($x = 0$ and 0.0075), their diffraction peaks were completely corresponding to the low-temperature α-Cu_2Se phase of the monoclinal structure (space group $C2/c$, PDF# 47-1448). In larger Cd original content sample ($x = 0.01$ and 0.02), the impurity phase of CdSe (PDF# 65-2891) was detected. The diffraction peak strength of the second phase of CdSe increased with the increase in Cd content in the raw material, indicating that the solubility of Cd in Cu_2Se was very low. The lattice parameters of all samples were refined by Rietveld, as shown in Fig. 2(b) and Table 1. When the original Cd content was low ($x = 0$ and $x = 0.0075$), the lattice parameters increased rapidly with the increase in the doping amount of Cd. The actual atomic percentage index that the solubility of Cd in Cu_2Se at room temperature was less than 0.6%. According to Shinnon radius data, Cd^{2+} ion radius (0.95 Å) is larger than Cu^+ ion radius (0.77 Å).[18] In the samples with low initial Cd content ($x = 0$ and $x = 0.0075$), the Cd atoms replaced the Cu atoms, and with the increase in original Cd content, it precipitated in a form of CdSe. The densities of all samples measured using the Archimedes method are shown in Table 1. The density of

samples with $x = 0$ and $x = 0.0075$ was very close to the theoretical value of Cu_2Se (6.74 g/cm^3), while that of samples with $x = 0.01$ and $x = 0.02$ was slightly less than the theoretical density of Cu_2Se (6.74 g/cm^3) for the low-density phase of CdSe (5.81 g/cm^3) existing in the sample.

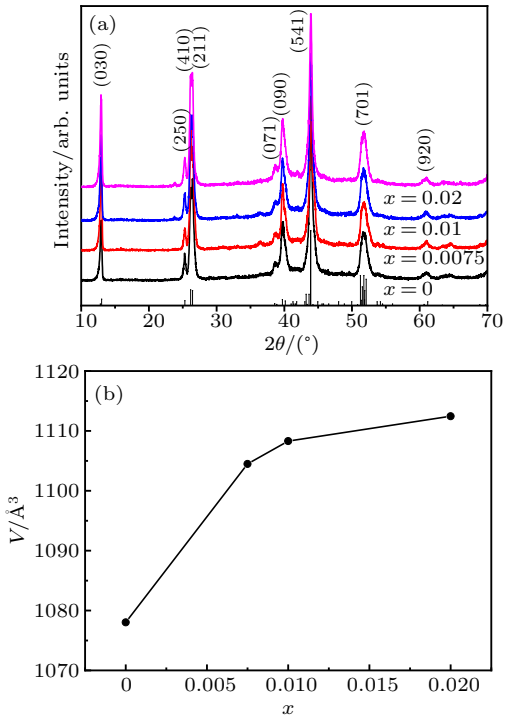


Fig. 2. (a) XRD patterns of samples prepared from different Cd starting materials and (b) cell volume of samples.

Table 2 lists the actual composition of all samples analyzed via EPMA. The content of Na and Cl atoms in all the samples was lower than 0.01%, indicating that these atoms were almost absent in the crystal. The sample was mainly composed of Cu, Se, and Cd. As the Cd content in the $x \leq 0.01$ sample increased, the Cd content in the sample also increased, whereas the Cu content decreased, indicating that Cd atoms replaced Cu atoms. However, when x continued to increase, no significant change was found in the Cd content in the sample, indicating that the Cd in Cu_2Se reached the limit of dissolution. The excess Cd and Se were combined to form the second phase of CdSe in the sample, which was consistent with the results of XRD analysis.

Figures 3(a) and 3(b) show the SEM images with 4×10^3 magnifications of $x = 0.0075$ and 0.02, respectively. No microscopic holes, cracks, nor grain boundaries were found in the sample of $x = 0.0075$, indicating that Cu_2Se-based materials prepared via NaCl flux method had good crystal quality. The second phase of CdSe was not observed in the sample with $x = 0.0075$ but distributed in the sample with $x = 0.02$, which was consistent with the results of EDS in Fig. 4. Figure 3(b) presents the FESEM micrographs of the fracture surface of the sample with $x = 0.0075$. The arranged lamellae formed a large-scale layered structure with an average thickness of approximately 100 nm, *i.e.*, layer and plane. These thinner lamellar crystals contained increased grain boundaries, which could scatter the phonon effectively, thus resulting in decreased . To determine the samples' lattice structure characteristics, the sample with $x = 0.02$ was analyzed using TEM. Figure 3(d) shows the HRTEM of the $x = 0.02$ sample, which was magnified 800 k times at an accelerating voltage of 200 kV. As shown in Fig. 3(c), the sample had good crystallinity and no obvious lattice defects. TEM images also showed that doping of Cd atoms did not destroy the crystal integrity of Cu_2Se. Therefore, doping Cd atoms formed displacement impurities in the crystal. The corresponding SAED pattern could be indexed as the [111] region axis. The measured lattice spacing of 0.35 nm corresponded to the lattice spacing in the {211} direction, and it was larger than the lattice spacing of α-Cu_2Se,[19] which may be attributed to the expansion of the lattice caused by the addition of Cd. These lattices of TEM, combined with the microstructures shown in the SEM images, are favorable for the low lattice thermal conductivity.

Table 1. Lattice parameters refined by Rietveld and density ρ of all samples.

Samples (Cu_{2-x} Cd_xSe)	a/Å	b/Å	c/Å	β/(°)	V/Å^3	ρ/g·cm^{-3}
$x = 0$	13.657	20.405	3.869	88.684	1078.03	6.71
$x = 0.0075$	13.678	20.585	3.918	90.192	1103.01	6.66
$x = 0.01$	13.885	20.244	3.962	85.372	1109.30	6.35
$x = 0.02$	13.683	20.380	4.057	90.168	1112.45	6.23

Table 2. Elemental compositions, Hall coefficients R_H, carrier concentration n, carrier mobility μ_H, and effective mass m^* at room temperature.

Samples	Chemical compositions					$R_H/10^{-2}$ m^3·C^{-1}	$n/10^{20}$ cm^{-3}	μ_H/cm^2·V^{-1}·s^{-1}	m^*/g
$Cu_{2-x}SeCd_x$	Cu	Se	Cd	Na	Cal				
$x = 0$	65.711	34.286	0	0.002	0.001	0.81	7.71	11.97	3.288
$x = 0.0075$	65.242	34.445	0.312	0.001	0	1.05	5.95	12.84	3.647
$x = 0.01$	64.627	34.807	0.564	0	0.002	1.53	4.08	14.32	3.224
$x = 0.02$	64.214	35.196	0.586	0.003	0.001	2.47	2.53	15.97	2.738

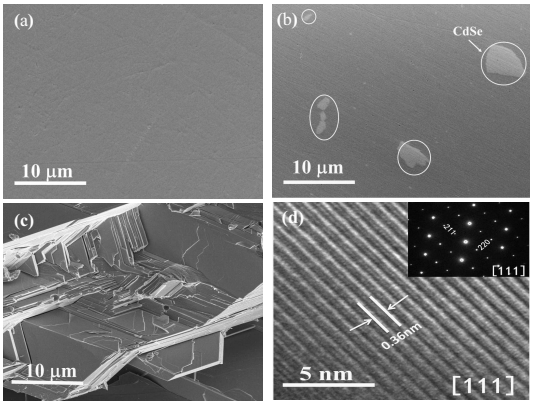


Fig. 3. (a) SEM figure of the sample $x = 0.0075$; (b) SEM of $x = 0.02$ sample; (c) FESEM of $x = 0.0075$ sample; (d) HRTEM and SAED pattern of the sample $x = 0.0075$.

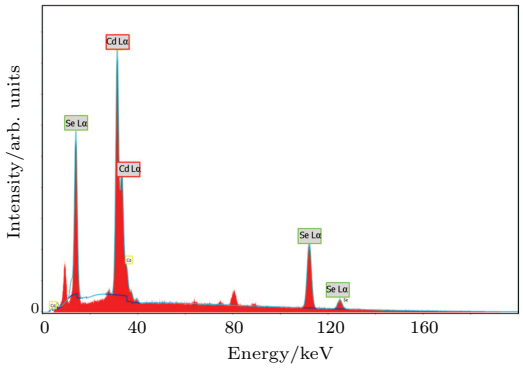


Fig. 4. The EDS spectrum of the region circled by the sample $x = 0.02$.

3.2. Electrical transmission characteristics of the samples

The temperature dependence of σ for all samples is presented in Fig. 5(a). In the whole temperature range, the conductivity of all samples was in the range of 10^4 S/m–10^5 S/m. These conductivities tended to decrease along with temperature increase, except for the phase transition point (approximately 400 K) showing a degenerated semiconductor behavior. Among them, the conductivity of unadulterated samples was slightly higher than that of the samples prepared via traditional hot-pressing method[20] and SPS[21] technology, possibly because of the different chemical compositions of the samples brought by the different starting materials and preparation methods. In addition, at a specific temperature, the conductivity decreased with the increase in Cd content. When $T = 300$ K, the conductivity decreased successively from 14.6×10^4 S/m to 6.4×10^4 S/m.

Hall tests were conducted on the samples at room temperature and carrier concentration and mobility were calculated in accordance with $n = \sigma/e\mu_H$ and $\mu_H = |R_H|\sigma$ to understand the electrical transmission characteristics of the samples, as shown in Table 2 and Fig. 5(b). The Hall coefficients of all samples were positive, indicating that all samples were P-type conductive. With the increase in Cd content, the carrier concentration decreased gradually and the carrier mobility increased gradually. When the Cd content was low, the Cu atoms were replaced by some Cd atoms. Cd^{2+} could provide more valence electrons than Cu^+ to reduce the concentration of hole carriers. Meanwhile, point defects and lattice distortion caused by Cd atom substitution on Cu atoms could effectively weaken the scattering between carriers and lead to increased carrier mobility. When the original Cd content continued to increase, a part of Cd^{2+} replaced Cu^+ and dissolved into Cu_2Se crystal, and some Cd^{2+} combined with Se^{2-} to form the second phase of CdSe. The presence of the second phase of CdSe increased the scattering between carriers. When the solid solubility of Cd atom reached saturation, the second phase of CdSe increased, while the carrier concentration and mobility rate tended to be flat.

The temperature dependence of α for all samples is presented in Fig. 5(c). The Seebeck coefficients of all samples were positive, indicating that the samples were P-type semiconductors, which was consistent with the Hall test results. In general, the Seebeck coefficient of the material increases with the decrease in carrier concentration and obviously increases with the increase in Cd content at a specific temperature. At 700 K, the Seebeck coefficient of the sample with $x = 0.02$ was 286 μV/K, which was significantly larger than that of the Pb-doped sample ($\alpha \approx 175$ μV/K at 700 K).[22]

In accordance with the measured conductivity and Seebeck coefficient, the power factor of all samples was calculated using the formula $PF = \alpha^2\sigma$, as shown in Fig. 5(d). The maximum power factor of the sample with $x = 0.0075$ at 700 K was 1.8×10^{-3} W·m^{-1}·K^{-2}, which was larger than that of the Pb-doped sample.[22] (1.1×10^{-3} W·m^{-1}·K^{-2}). Such an evident enhancement in the power factor is attributed to the strongly enhanced Seebeck coefficient and less affected electrical conductivity. In order to find out the high PF value of $x = 0.0075$ at high temperature, we tried to measure the high temperature Hall. However, at high temperatures, for Cu_2Se with low mobility, the Hall can be difficult or even not possible to measure. The weighted mobility can be thought of as a non-degenerate value for mobility which should better for analyzing small changes in band structures with alloying.[23] This approach for evaluating weighted mobility could be especially helpful in analyzing the transport in materials like $Cu_{2-x}Se$ where it is not straightforward to interpret (or sometime hard to obtain) Hall measurements at high temperatures.[24] The weighted mobility is preferable to Hall mobility for Cu_2Se. The results in Fig. 6 show that the weighted mobility of sample $x = 0.0075$ is slightly higher than other samples at high temperature. At the same time, for all samples, the effective mass of the state density does not change much at room temperature, as shown in Table 2. The above results show that the high PF of $x = 0.0075$ is mainly due to the optimization of carrier concentration, and the band effect is less affected. This result showed that the Cu_2Se prepared by doping proper Cd could optimize the power factor.

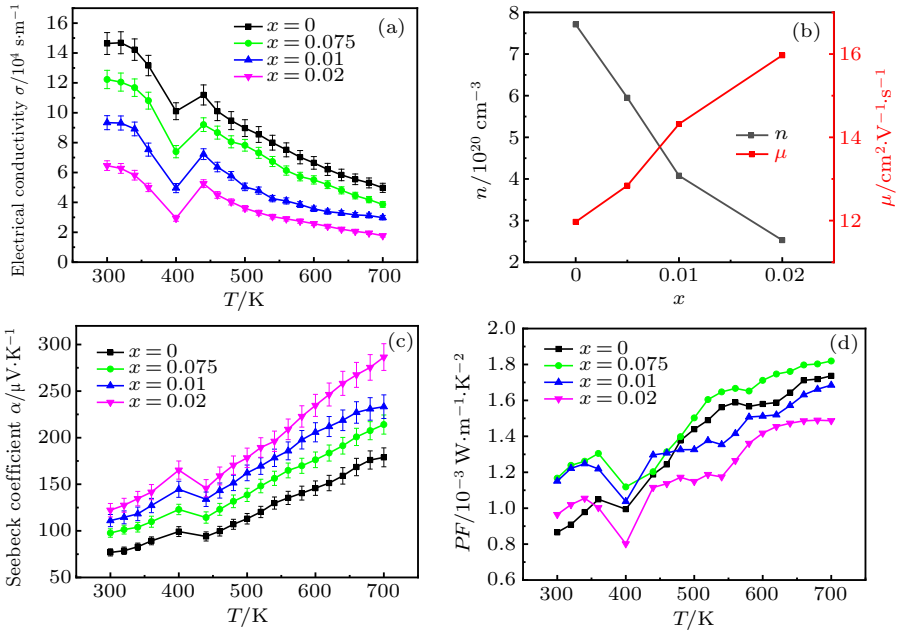


Fig. 5. Measured temperature-dependent thermoelectric properties of all the samples: (a) σ, (b) n and μ, (c) α; (d) PF.

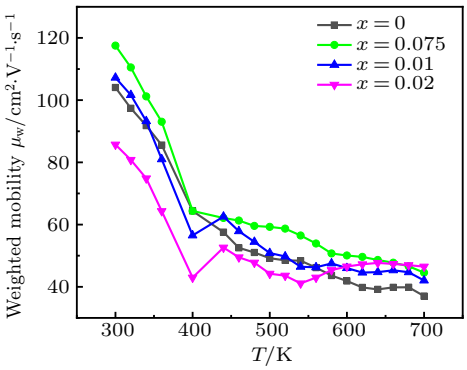


Fig. 6. Weighted mobility, evaluated from the thermopower and conductivity data, as a function of temperature.

3.3. Thermal conductivity and *ZT* values

The temperature dependence of the specific heat capacity for all samples is presented in Fig. 7(a). Corresponding to the conductivity and Seebeck coefficient, the specific heat capacity of all samples increased sharply near the phase transition point of 400 K. The phase transition points were 407 K, 412 K, 413 K, and 413 K, which were all close to the phase transition temperature of Cu_2Se (396 K $\pm$ 15 K). In general, an increase or decrease in C_p of a material corresponds to an increase or decrease in the degrees of atomic freedom within its structure.[14] This case implied that the atomic motions, such as atomic vibration, in the Cu_2Se structure and the diffusivity of Cu^+ ions within the crystal lattice decreased in the samples with $x = 0.01$ and 0.02. This result further supported the fact that these exhibited decreased mobility when the original Cd content was high. Moreover, the reason why the phase transition points of the samples with $x = 0.01$ and 0.02 were slightly higher than those of undoped samples may be related to the presence of the second phase of CdSe. The temperature dependence of the thermal conductivity for all samples is presented in Fig. 7(b). The thermal conductivity showed a decreasing trend with the increase in temperature, except near the phase transition point where, it increased sharply. In the whole temperature range, the thermal conductivity of the samples with $x = 0.0075$ was slightly lower than that of the undoped sample. At the temperature of 300 K, the lowest thermal conductivity was approximately 0.8 W·m^{-1}·K^{-1}, which was equivalent to that of the Pb-doped sample ($\sim$ 0.85 W·m^{-1}·K^{-1}).[22] The thermal conductivity of the samples with $x = 0.01$ and $x = 0.02$ increased sharply compared with that of the unadulterated samples, possibly due to the formation of the second phase of CdSe in the samples. The of all samples was calculated, as shown in Fig. 7(c). For Cd-doped samples, the solid dissolved Cd atoms significantly reduced the of the material because lattice distortions and defects effectively enhanced phonon scattering. The lattice thermal conductivity (κ_L) was calculated using $\kappa_L = \kappa - \kappa_e$, where was calculated using (L is the Lorenz number). However, for the samples with $x = 0.01$ and $x = 0.02$, κe decreases due to a sharp decrease in electrical conductivity, leading to an increase in κ_L. Therefore, the sample with $x = 0.0075$ was obtained the minimum κ_L.

The ZT values of all samples were calculated, as shown in Fig. 7(d). For the highest power factor and the lowest thermal conductivity, the sample with $x = 0.075$ exhibited the best thermoelectric performance, and its maximum ZT value reached 1.67 at 700 K, higher than that of the Pb-doped samples (approximately 0.7 at 700 K).[22] ZT enhancement could be attributed to the very low κ and good PF, which benefits from the strong phonon scattering by high-density grain boundaries and nanoscale structure engineering. Under the same temperature, this value was also higher than that of the Ag-doped samples (approximately 0.53)[9] and the Ni-doped samples (approximately 1.0). For the existence of CdSe, the thermal conductivity of the samples with $x = 0.01$ and $x = 0.02$ was significantly higher than that of the undoped samples, re-

sulting in a lower ZT value than that of the undoped samples. In addition, the ZT value increased steadily as the temperature increased, indicating that this value was higher when the temperature was above 700 K.

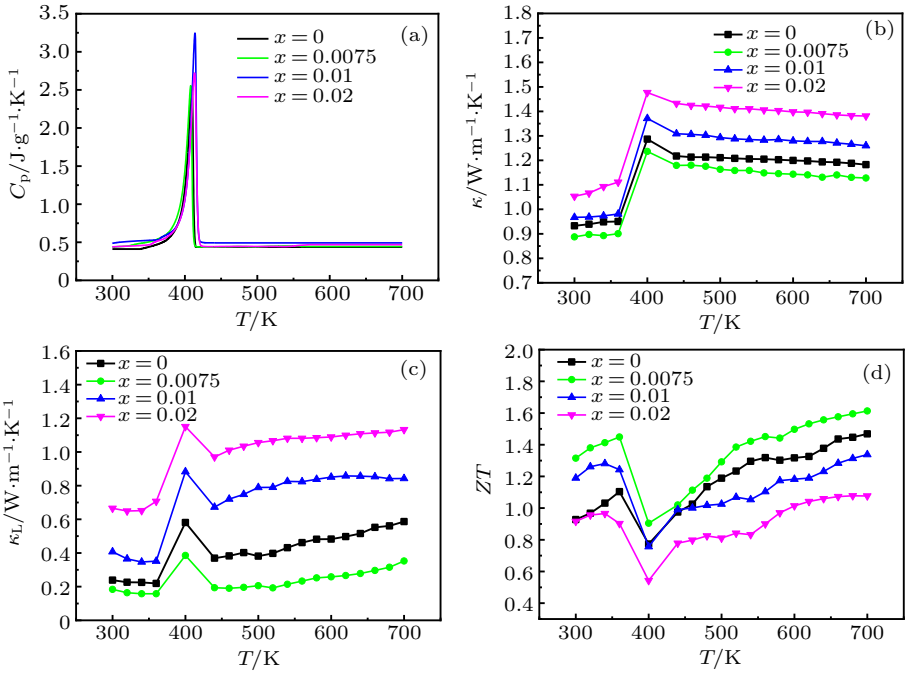


Fig. 7. Thermal transport performance parameters of all samples related to temperature T: (a) C_p; (b) κ; (c) κ_L; (d) ZT.

3.4. Thermal stability

Poor thermal stability is the main issue preventing the practical application of Cu_2Se. Figure 8 shows the temperature dependence of the TG–DTA curves for all samples. The TG curve illustrated that the weight loss of all samples was hardly detected below the temperature of 1450 K. This result showed that the Se volatilization in Cu_2Se samples prepared via NaCl flux was inhibited. The DTA curve indicated an endothermic peak at approximately 1418 K, which was slightly higher than the melting point of 1403 K shown in the CuSe phase diagram.[25] Figures 8(a)–8(d) show endothermic peaks at approximately 407 K, 412 K, 413 K, and 413 K. This finding was coincidental with the phase transition temperature. The increase in phase transition temperature in Cd-doped Cu_2Se could be attributed to the introduction of Cd in the lattice, which had increased atomic mass and radius, there by enhancing the thermal stability by blocking Cu diffusion.

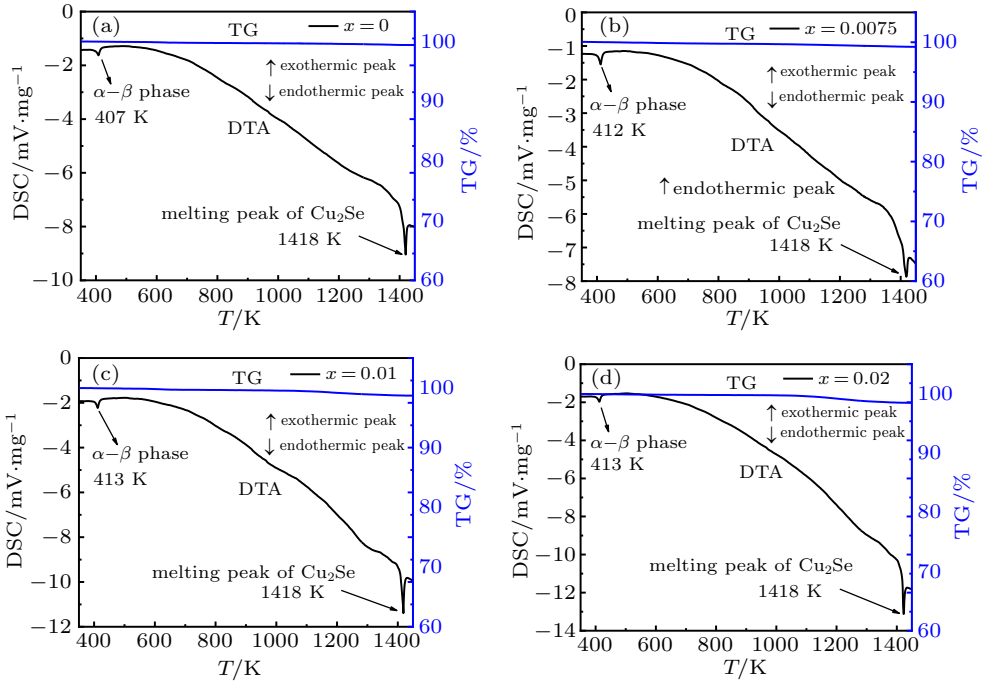


Fig. 8. TG–DTA curves for all samples performed in an open alumina crucible with a heating rate of 10 K/min: (a) $x = 0$; (b) $x = 0.0075$; (c) $x = 0.01$; (d) $x = 0.02$.

4. Conclusions

In this study, nano-layered Cu_2Se thermoelectric materials with excellent crystal quality and high ZT values were prepared using the NaCl-flux method on the basis of the stoichiometric ratios of $Cu_{2-x}SeCd_x$ ($x = 0$, 0.0075, 0.01, and $x = 0.02$). XRD results showed that the diffraction peaks of the samples were completely corresponding to the low-temperature α-Cu_2Se phase of the monoclinal structure. When the initial Cd content was large ($x = 0.01$ and $x = 0.02$), the impurity phase of CdSe was detected in the sample. EPMA showed that the solubility of Cd in Cu_2Se at room temperature was less than 6%. TEM indicated that doping Cd atoms did not destroy the crystal integrity of Cu_2Se. Besides, with the increase in Cd content in the sample, the carrier concentration decreased gradually and the mobility increased gradually. However, excessive Cd doping led to the emergence of a second phase of CdSe in the sample. Eventually, the sample with $x = 0.075$ showed the best thermoelectric performance among all the samples. The maximum ZT value of 1.67 was obtained at 700 K. This work demonstrated that the thermoelectric properties and thermal stability of materials could be further optimized by doping an appropriate amount of Cd into nanoscale Cu_2Se compounds.

References

[1] Zhu Z, Zhang Y, Song H and Li X J 2018 *Appl. Phys. A* **124** 1
[2] Tang Y, Li D, Chen Z, Deng S, Sun L, Liu W, Shen L and Deng S 2018 *Chin. Phys. B* **27** 118105
[3] Seebeck T J 2010 *Annalen Der Physik* **82** 133
[4] Liu H X, Deng S P, Li D C, Shen L X and Deng S K 2017 *Chin. Phys. B* **26** 027401
[5] Liu W, Shen L, Shai X, Sun L, Lu J, Chen J, Ge W and Deng S 2019 *CrystEngComm* **21** 6850
[6] Toberer E S, Zevalkink A and Snyder G J 2011 *J. Mater. Chem.* **21** 15843
[7] Gahtori B, Bathula S, Tyagi K, Jayasimhadri M, Srivastava A K, Singh S, Budhani R C and Dhar A 2015 *Nano Energy* **13** 36
[8] Liu H, Shi X, Xu F, Zhang L, Zhang W, Chen L, Li Q, Uher C, Day T and Snyder G J 2012 *Nat. Mater.* **11** 422
[9] Ballikaya S, Chi H, Salvador J R and Uher C 2013 *J. Mater. Chem. A* **1** 12478
[10] Zhong B, Yong Z, Li W, Chen Z, Cui J, Wei L, Xie Y, Hao Q and He Q 2014 *Appl. Phys. Lett.* **105** 123902
[11] Zhao K, Blichfeld A B, Eikeland E, Qiu P, Ren D, Iversen B B, Shi X and Chen L 2017 *J. Mater. Chem. A* **5** 1
[12] Zhao L, Nazrul Islam S M K, Wang J, Cortie D L, Wang X, Cheng Z, Wang J, Ye N, Dou S and Shi X 2017 *Nano Energy* **41** 164
[13] Nunna R, Qiu P, Yin M, Chen H, Hanus R, Song Q, Zhang T, Chou M Y, Agne M T and He J 2017 *Energy Environ. Sci.* **10** 1928
[14] Olvera A A, Moroz N A, Sahoo P, Ren P, Bailey T P, Page A A, Uher C and Poudeu P F P 2017 *Energy Environ. Sci.* **10** 1668
[15] Wang L, Chang S, Zheng S, Fang T, Cui W, Bai P P, Yue L and Chen Z G 2017 *Acs Appl. Mater. Interfaces* **27** 22612
[16] Khot K V, Mali S S, Pawar N B, Kharade R R, Mane R M, Patil P B, Patil P S, Hong C K, Kim J H and Heo J 2015 *Rsc Adv.* **5** 40283
[17] Ved, Vati, Singh, Ajai and Kumar 2015 *Dalton Transactions* **44** 725
[18] Shannon R D 1976 *Acta Crystallographica Section A Foundations of Crystallography* **32** 751
[19] Lei Y, Chen Z G, Han G, Min H, Huang L and Jin Z 2016 *J. Mater. Chem. A* **4** 9213
[20] Shi D, Geng Z and Lam K 2019 *Energies* **12** 401
[21] Zou L, Zhang B P, Ge Z H and Zhang L J 2014 *Funct. Mater. Lett.* **29** 1047
[22] Zhu Z, Zhang Y, Song H and Li X J 2018 *Appl. Phys. A* **124** 871
[23] Snyder G J, Snyder A H, Wood M, Gurunathan R, Snyder B H and Niu C 2020 *Adv. Mater.* **20** 2001537
[24] Kang S D, Pöhls J H, Aydemir U, Qiu P, Stoumpos C C, Hanus R, White M A, Shi X, Chen L, Kanatzidis M G and Snyder G J 2017 *Mater. Today Phys.* **1** 7
[25] Chakrabarti D J and Laughlin D E 1981 *Bulletin of Alloy Phase Diagrams* **2** 305